Operando photoelectron emission spectroscopy and microscopy at Elettra soft X-ray beamlines: from model to real functional systems

M. Amati[1], L. Bonanni[2], L. Braglia[2], F. Genuzio[1], L. Gregoratti[1], M. Kiskinova[1*], A. Kolmakov[3], A. Locatelli[1], E. Magnano[2], A. A. Matruglio[1,2], T. O. Menteş[1], S. Nappini[2], P. Torelli[2], P. Zeller[1]

[1] Elettra-Sincrotrone Trieste S.C.p.A, Area Science Park, 34149 Basovizza, Trieste, Italy

[2] CNR-IOM, TASC Laboratory, 34149 Trieste, Italy

[3] Center for Nanoscale Science and Technology, NIST, Gaithersburg, MD 20899, USA

- Corresponding author: maya.kiskinova@elettra.eu

Abstract: Implementation of in-situ and operando experimental set-ups for bridging the pressure gap in characterization techniques based on monitoring of photoelectron emission has made significant achievements at several beamlines at Elettra synchrotron facility. These set-ups are now operational and have been successfully used to address unsolved issues exploring events occurring at solid–gas, solid–liquid and solid-solid interfaces of functional materials. The sections in the article communicate the research opportunities offered by the current set-ups at APE, BACH, ESCAmicroscopy and Nanospectroscopy beamlines and outline the next steps to overcome the present limits.

1. Introduction

Shedding light on the evolving physical and chemical properties of smart materials and devices during their fabrication, processing and operation is one of the main challenges in revealing which are the essential ones for their functionality and durability. In this respect multimodal spectroscopic analyses with elemental, electronic and structural sensitivity, spanning a wide spatiotemporal range, provide unique fundamental information related to the emerging functional properties we seek.

Inherent feature of all functional systems is the presence of solid/solid, solid/gas and/or solid/liquid interfaces playing essential roles in the operational mechanisms. They include numerous reaction and transport steps as atom or charge transfer, chemical reactions by exposing to various environments, mass transport, phase transitions etc. In-situ probing how the interfacial structure and functionality responds to external stimuli or changes in the chemical composition is still a cross-cutting research challenge. Judging from the number of publications, among the most extensively studied functional systems are relevant to heterogeneous catalysis, that is keystone of chemical industry, fuel and energy production, conversion and storage and also crucial part of the devices for environmental protection. The complexity of these systems is multilevel and needs monitoring evolutions in properties, modifications or degradation of the catalysts and all other essential building blocks as catalyst supports, electrodes, electrolytes, gas or liquid ambient etc. during operation.

Another open questions are relevant to operation principles of ultra-fast devices that requires to uncover how the intense light, electric and magnetic fields can drive such systems into a desired state and how we can use the non-equilibrium routes to influence their functionality.

In the last decade one of the key leaders in development of appropriate in-situ/operando tools with spectral, lateral and time resolution, matching the sizes and functions of the matter under investigation, are the large scale synchrotron research centers. The great advantage of using synchrotron light in developing advanced methodologies that have made possible the transition from model to real systems is the ability to select the photon parameters that allow experiments with spectroscopies providing the desired spectral, depth and lateral information. The main limiting factors for operando experiments are the photon wavelength and detected signal. The penetration-information depth of photon-in/photon-out techniques, as X-ray emission spectroscopy (XES), resonant inelastic X-ray spectroscopy (RIXS) and X-ray Absorption Spectroscopy (XAS) in transmission or fluorescence yield mode, exceeds 100 nm, whereas the information depth of photon-in/electron-out X-ray Photoelectron Spectroscopy (XPS) and XAS in total or partial electron yield is limited to less than 10 nm. Apparently, the experiments based on monitoring the photoelectron emission are surface

sensitive and, in principle, not applicable to non-conducting samples. The short electron inelastic mean free path (IMFP) also requires vacuum that imposes the so-called pressure gap problem for operando experiments. However, the surface sensitivity of photon-in/electron-out experiments is a great advantage for investigations of interfacial phenomena that relate directly to the performance of catalysts, electrochemical energy devices, sensing and many other electronic devices.

Various experimental set-ups have already been developed in synchrotron laboratories worldwide and are described recently in dedicated special issues of some journals [1] and review articles, see e.g. ref. [2, 3, 4, 5]. In this paper we report the present achievements and on-going activities at Elettra synchrotron facility with focus on the set-ups overcoming the limits imposed by photon-in/electron-out experiments. This is the first report that puts together developments at several Elettra beamlines, where each section describes the used operando approaches with selected results representing the offered research opportunities.

2. Environmental cell for operando soft X-ray absorption spectroscopy in total electron yield mode

As notified in the introduction detection of electrons imposes more limits to the sample environment. Since the photon penetration depth and IMFP of the emitted electrons depend on their energy using hard X-rays simplifies to a certain extend the development and implementation of *operando* set-ups that have already become rather common. However, along with the lower sensitivity in the XPS experiments, this is at the expense of the limited access in XAS mode to very essential electron edges, in particular K-edges of light elements as B, C, O, N. The latter are key constituents of the 2D materials (graphene, BN), functional materials as metal oxides and majority of the species (molecules and atoms) that are involved in catalytic reactions and the evolution of their XAS spectra under operation reveals simultaneously the undergone electronic and structural changes. Further-on the $L_{2,3}$-edges of the first row transition metals provide crucial information about unoccupied *s*- and *d*- density of states (DOS), complementing the K-edge XAS obtained using hard X-rays, which is exclusively probing unoccupied *p*-DOS. The information about the presence and occupation of molecular orbitals provided by the *d*- DOS is of particular importance in comprehension the nature of the chemical bonds of an active metal site with the ligands at the interfaces and the chemical modifications undergone under working conditions. In addition, the comparison of the L_2 and L_3-edge signals also provides information on the role of the spin in the chemical bond, which cannot be obtained from the K-edges XAS. However, using soft X-rays one has to solve more severe problems imposed by the more stringent vacuum, transparency and mechanics constraints.

In the present section we describe the construction and performance of a new environmental cell for *in-situ*/in-*operando* XAS experiments in total electron yield (TEY) mode measuring the drain current from the sample and using photon energies in the range 150-1600 eV. This set-up is available at the experimental station of APE-HE beamline at Elettra synchrotron [6]. Its design is based on the long experience from soft X-ray microscopy experiments where the transparent to the X-rays Si_3N_4 windows have regularly [7] been used since they also resist the synchrotron radiation that secures long life time of the Si_3N_4 sealed environmental cells. At present two ambient pressure devices are operational: one is already described in ref. [8]. Recently, we have developed a new cell, which, as reported below, can also be operated during heating the sample to 350°C.

It should also be notified that monitoring XAS in TEY mode ensures relatively large signal and a pronounced surface sensitivity that does not exceed 10 nm in the worst cases, which makes the set-up very appropriate for exploring interfacial phenomena. An essential feature of this piece of equipment is that it routinely works in the soft X-ray range in a gas ambient of 1 bar (often mixed with He) that to certain extend reduces the undesired charging of low-conductive samples [9], the main limitation using TEY since it shifts the spectra and reduces the signal intensity. Another solution to handle charging issues is mixing insulating specimen with conductive inert species (e.g. C) or using very thin films grown on conducting material.

Figure 1 (a, b) shows a cross-section drawing and a sketch of the reactor cell divided in its constituent parts, respectively. The cells are manufactured of Ti that is chosen for its chemical inertness. Ultrathin Si_3N_4 membranes are used as windows for penetration of the X-ray beam and as a seal of the atmospheric sample ambient, which makes the cell fully compatible with the ultrahigh vacuum requirements of the beamline and spectroscopy end station. Two PTFE (polytetrafluoroethylene) pipes allow feeding the cell volume with different types of gases for exploring the response of the sample hosted inside the cell. For recording XAS in TEY mode we monitored with a picoammeter the drain current from the sample while scanning the X-ray energy. The high signal-to-noise ratio achievable in the TEY mode makes possible obtaining XAS spectra with good statistics in a few seconds.

The performance and the research opportunities opened by this type environmental ambient pressure cells at beamline APE are demonstrated by representative, recently obtained results reported in Figure 1. In the first ambient pressure study reported in [10] we explored the solvatochromic effect of a Fe-based spin-crossover (SCO) compound. The molecule under investigation is 2-(pyrazol-1-yl)-6-(1H-tetrazol-5-yl)pyridine (see the structure reported in the inset of Fig. 1c). Comparing the Fe $L_{2,3}$ XAS spectra in Fig. 1c, measured at room temperature (RT) and 1 bar He or CH_3OH/He ambient, one can see the distinct differences in the relative intensity of the spectral features at 713 eV and 715 eV. This result reveals that the adsorption of methanol, which binds to the iron induces a change of the spin state of the Fe(II) atoms from low spin to high spin. As evident in Fig. 1c, the process is reversible – altering from CH_3OH/He feed to He feed the Fe(II) $L_{2,3}$ spectrum restores the He-characteristic features.

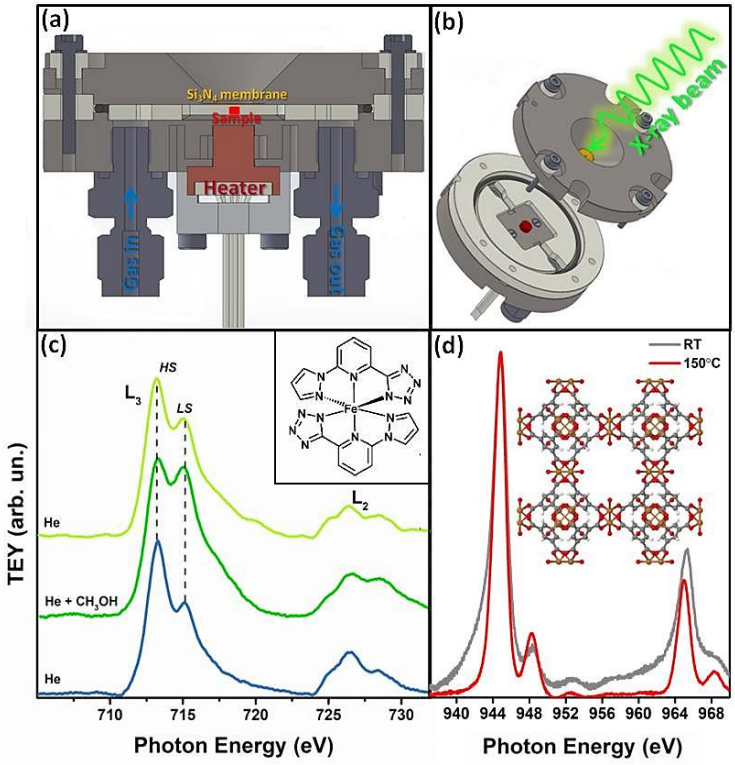

Figure 1. (a) Cross section sketch and (b) main components of the cell for XAS measurement in TYE mode at APE-HE beamline. (c) Fe (II) $L_{2,3}$ XAS spectra of a SCO molecule (the molecule structure is shown in the inset) in He flux (blue line), CH_3OH/He flux (green line) and after switching the CH_3OH/He feed to He feed (light green) [8]. (d) Cu $L_{2,3}$ XAS spectra of the HKUST-1 sample (the molecule structure is shown in the inset) at RT (grey) and at 150°C (red).

The second example, reported in Fig. 1d), is one of the first experiments for testing the cell capabilities during sample heating. We used a HKUST-1 sample, a metal organic framework (MOF) that is among the

MOFs considered for applications in sensing, gas adsorption and separation, etc. [11,12,13,14]. This is porous material consisting of copper nodes with 1,3,5-benzenetricarboxylic acid interconnected between them (see the insert in Fig. 1d). We performed XAS experiments at the Cu $L_{2,3}$ edges at 1 bar He feed and RT and after annealing to 150°C that removes the adsorbed 'contaminant' molecules on the surface (water, organic solvent, etc.). The two Cu(II) XAS spectra in Fig. 1(d) clearly illustrate the improvement in the quality of the signal due to the effect of cleaning as a result of the thermal treatment. In principle, after this thermal cleaning the sample is ready for further possible treatments/interactions with gases that are of interest for specific applications.

3. Photoelectron spectroscopy in gas and liquid ambient using electron transparent membranes

In the last decade several solutions have led to success in bridging the so-called "pressure gap" between ultra-high vacuum surface sensitive methods based on direct electron detection such as XPS-AES, XAS in TEY, low energy electron microscopy (LEEM) and scanning electron microscopy (SEM). These solutions have overcome the major obstacles for in-situ operando investigations under realistic sample environments. Currently, the instrumentation at synchrotron light facilities for (near) Ambient Pressure Photoelectron Emission Spectroscopy (APPES) that comprises both XPS and XAS in total or partial electron yield evolves in two directions: (i) via development of the differential pumping stages coupled with sophisticated electron optics and/or sample delivery systems [15,16,17,18] and more recently, (ii) via implementation of electron transparent and molecularly impermeable membranes, such as graphene that separate the gaseous and liquid ambient of the sample from the UHV environment of the electron detector/analyzer [3, 19, 20, 21]. In particular, the implementation of the graphene liquid cells has made the ambient environment modifications of the analytical instrumentation to be redundant since all complexities of the electron collection and sample delivery can be resolved effectively employing existing lab-on-a-chip MEMS technologies [22].

For the construction of 'graphene sealed set-ups' one should consider several requirements and limitations that are detrimental for designs of the graphene liquid or ambient gas pressure environmental cells. The first is that the membrane thickness should be inferior than the electrons IMFP in dense media, λ, which depends on the kinetic energy of the electrons, e.g. λ ranges from one to several nm going from soft to harder x-rays excitation. Along with the acceptable membrane thickness the x-rays energy and corresponding kinetic energy of emitted electrons also determine the probing depth in the encapsulated specimen under investigation and the attenuation of the electron signal. Considering the compromise between two parameters - the fast drop of the photoionization cross sections of the most common elements of interest with increasing the photon energy and the concomitant increase of the electrons IMFP, for getting optimal electron emission signal the preferable x-ray excitation range for graphene membrane based environmental cells is within the range 800-2000 eV [23]. The latter overlaps well with the experimental capabilities at several spectroscopy beamlines at Elettra and the graphene membrane approach has already been implemented at three of them (ESCAMicroscopy, NanoSpectroscopy and BACH). In addition, one should consider that the finite mechanical strength of the graphene limits the size of the graphene windows, since only a few square microns of graphene can sustain 1 Bar pressure differential. This fact points up the importance of the dimensions of the X-ray (electron) beam probing the solid/gas and solid/liquid interfaces. That is why the first successful photon-in/electron-out experiments using with graphene sealed reaction cells were performed with the Scanning PhotoElectron Microscope (SPEM) operated at ESCAMicroscopy beamline, which uses zone plate focusing optics for providing submicrometer X-ray probe [24].

The designs of already developed and operating graphene sealed set-ups can generally be divided into four different types: single orifice cells [19, 25, 26, 27], graphene-capped isolated micro-volume arrays [22], common volume arrays [28, 29, 14] and graphene encapsulated samples [30, 31, 32, 33]. All these types of environmental cells can have either a close volume or fluidic designs.

Figure 2 summarized the principle design and components of two 'graphene-based' set-ups (Fig. 2a and c) and examples of the photoelectron spectra collected with SPEM using graphene liquid cells (Fig. 2b and d). Due to their simplicity in fabrication, single window graphene liquid cells (Figure 2a) were used first in the early SPEM studies of liquids. In particular, the process of x-ray induced water radiolysis was recorded *in situ* spectroscopically and reported in [19]. The later upgrades of the single orifice with working and counter electrodes resulted in XPS monitoring the metal plating process from aqueous electrolyte [3] (Fig. 1b), while more recent construction for similar cells, adding the input/output inlets, has allowed for liquid exchange behind the graphene [34]. The major disadvantage of the single window approach is the limited chemical durability of the graphene membrane exposed to photon-electron radiation during prolonged data acquisitions, which inspired the development of the multi-channel array (MCA) graphene cells (Fig. 2c). The MCA set-up platform has significantly enhanced the SPEM capabilities to probe multiple identical objects under operando conditions. This turned out to be of particular importance when time dependent undesired events, such as beam damage of the specimen or graphene membrane are present. Figure 2d shows a representative example of electrochemical SPEM study of electrified graphene-liquid electrolyte (0.1 M $CuSO_4$ aqueous solution) interface, using the MCA set-up. The evolution of the XPS spectra, collected through a bilayer graphene window (also acting as a working electrode), was monitored as a function of the bias at the counter electrode (CE). As can be seen the O 1s spectra mainly evolve as a function of the measurement time irreversibly and not really correlated with the CE potential. The fast attenuation of the liquid water component, O_{Liq}, and the irreversible growth of O^{2-} lower BE component are presumably related to the beam induced water splitting. The MCA graphene cells have the advantage that they can also be used in experiments with X-ray Photoelectron Microscopy (XPEEM) and LEEM. Such a design consisting of thousands of identical samples has also allowed for high throughput combinatorial data mining algorithms, such as principle component analysis, clustering, Bayesian inference methods, to be applied to analyze multi-dimensional/hyperspectral XPEEM datasets [20, 35].

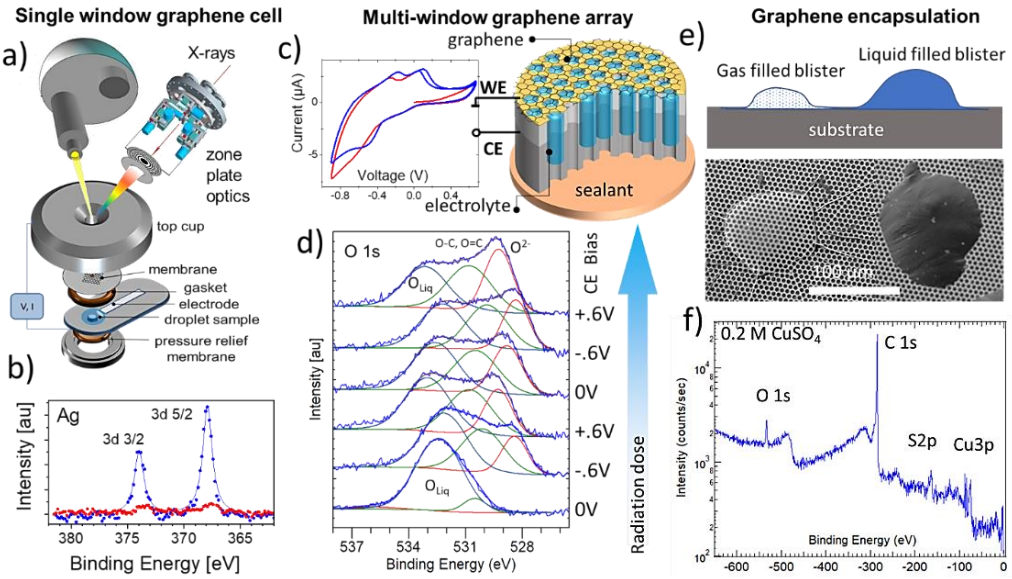

Figure 2 (a) Sketch of the main components of an environmental graphene-sealed cell that can also be used for electrochemical experiments (b) Ag 3d spectra recorded at the graphene membrane interfaced with AgNO3 solution that is (-)(blue) and (+) (red) biased with respect to the counter electrode [3] (c) MCA setup for through-the-membrane spectromicroscopy of liquids with option for applying potentials [20] (d) Consecutive O 1s spectra at different potentials - their evolution is apparently correlated mainly to acquisition time indicating the radiation-induced water splitting [21]. (e) Sketch of liquid encapsulation and the measured SEM images (f) XPS of encapsulated $CuSO_4$ solution.

Finally, the notable strength coupled with flexibility and appreciable adhesion of the single and multilayer graphene to many substrates opens the possibility to encapsulate liquid, gaseous or solid objects under the graphene and study them under real word or elevated pressure and temperature conditions. Figure 2e) depicts high vacuum SEM image of water vapor and $CuSO_4$ aqueous solution pockets captured under multilayer graphene and Fig. 2f) demonstrates the feasibility to collect good quality XPS spectra of underlying liquid even through 4-6 layers of graphene.

Due to its relative simplicity, the direct encapsulation approach is very attractive and has already resulted in breakthrough spectroscopic studies of gases under ultrahigh pressures, (photo-) catalysis research under confined conditions and biomedical objects [30, 31, 32, 33]. One of the first demonstrations of the resistance of graphene to extreme gas pressures was made using XPEEM encapsulating noble gas under graphene grown on a metal substrate [32].

The research interests relevant to studies in liquid environment, as comprehension of electron transfer processes at the solid/liquid interfaces during physico-chemical processes, such as photo-catalysis or electrochemistry, does not always require microscopic approach. Using photon beam dimensions of the order 50-200 by 100-300 μm at typical spectroscopic beamlines one can obtain a lot of useful information collecting the signal from a number of encapsulated nanodroplets. This has allowed implementation of the direct encapsulation set-up at BACH beamline [36] where both XPS and XAS measurements are used for providing information on the electronic structure and chemical properties of the constituents at solid/liquid interfaces [30].

The experimental set-up developed at the BACH beamline for studying liquid-solid interfaces is based on the transfer in liquid environment of graphene membranes on the surface of solid samples of interest. This transfer method is reproducible and the encapsulation of the liquid between the graphene membrane and the solid sample allows spectroscopic characterization of the liquid/solid interphase. This liquid encapsulation procedure was applied for the first time in studies of a TiO_2 sample, an excellent photocatalyst with a great variety of applications, e.g. water purification, photo-degradation, water splitting [37, 38, 39, 40]. However, all these systems still lack complete comprehension of the phenomena governing the relevant interfacial processes.

The morphology of the graphene-encapsulated aqueous solution between the graphene layer and TiO_2(100) rutile single crystal on a fresh prepared sample and after a subsequent annealing to 350°C was examined first using scanning tunneling microscopy (STM). STM results showed that the graphene membrane transfer at room temperature (RT) has led to trapping of the solution in the form of randomly distributed 'graphene' nanobubbles (GNBs) of various shapes with an average height of 6 nm and dimensions of the order of hundreds nm. The following annealing led to a collapse the GNBs resulting in formation of more uniform encapsulated liquid layer. These STM results demonstrated that formation and evolution of the GNBs on TiO_2 open the great opportunity to use soft x-ray spectroscopies for exploring the thermal-induced processes as temperature-induced reduction of $FeCl_3$ [30] and the photo-reduction mechanism of Prussian Blue (PB soluble form, $KFe^{III}[Fe^{II}(CN)_6]$) [41].

In the first study we followed in-situ the reaction occurring upon annealing of the GNBs encompassing the $FeCl_3$ solution up to 250°C. We measured the Fe 2p, O 1s and Cl 2p core level spectra with high resolution hemispherical electron analyzer and the corresponding L- and K- XAS by monitoring the drain current directly on the graphene membrane while scanning the photon energy. As illustrated in the panels in Fig. 3 (a) the liquid water component at 533.5 eV in the O 1s spectrum, the component of the Cl^- ions in solution at 200.3 eV in the Cl 2p spectrum and the Fe $L_{2,3}$-edge XAS spectrum are excellent fingerprints for following the evolution of the aqueous $FeCl_3$ solution upon annealing. At RT the Fe L-edge XAS spectrum shows the main features characteristic for Fe^{3+}, as confirmed by the Ligand Field Multiplet simulations. Upon annealing both the O 1s and Cl 2p XPS spectra and the Fe L-edge XAS evidence the occurrence of thermal reduction from $FeCl_3$ to $FeCl_2$. The changes of the Fe L-edge XAS result in appearance of typical features expected for $FeCl_2$

(well reproduced by the simulation of Fe^{2+}), whereas the decrease of the O 1s liquid water component and the increase of the Cl 2p intensity are in agreement with the chemical evolution evidenced by XAS and the morphology changes evidenced by STM upon annealing when the bubbles convert to a flat rather uniform in height liquid layer.

In the second study we were able to monitor the photo-induced reduction of Fe^{3+}–N → Fe^{2+}–N from Prussian blue (PB) to Prussian white (PW) in aqueous solution by using the same graphene encapsulated liquid procedure. For exploiting the photocatalytic properties of TiO_2 upon UV excitation the GNBs formed on the TiO_2 single crystal represented both "sample container" and "reactor" allowing for in-situ following the reaction processes. In these experiments the Fe $L_{2,3}$ XAS spectra were measured in TEY mode by the electron analyzer, thanks to the sufficient electron transparency of the graphene membrane. As shown in Fig. 3(b) the evolution of the Fe $L_{2,3}$ XAS spectra clearly reveals the electron PB to PW reduction. The same exposure to UV, performed on a dried sample prepared by drop-casting method on TiO_2 rutile single crystal, does not show any feature of reduced Fe. The obtained results with graphene encapsulated solution unequivocally demonstrates that the reaction occurs preferentially in aqueous ambient, where water acts as hole scavenger preventing the electron recombination process.

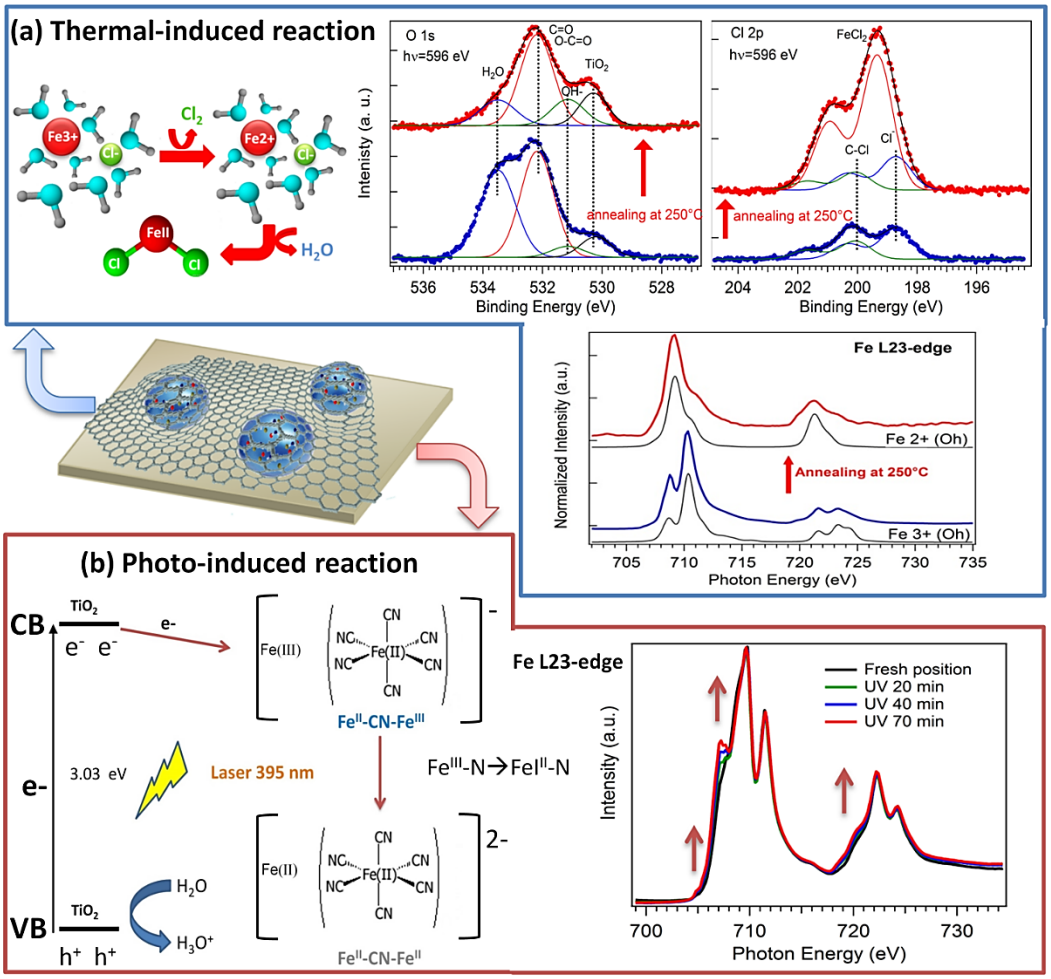

Figure 3: (a) Thermal induced reduction of $FeCl_2$ aqueous solution confined in GNBs revealed by the evolution of the O1s and Cl 2p XPS spectra Fe L_{23} XAS spectra evidencing the reduction from Fe^{3+} to Fe^{2+} induced by annealing to 250°C [28]. (b) Photoinduced reduction of PB aqueous solution confined in GNBs where the FeL_{23} XAS spectra upon UV band gap excitation of TiO_2 demonstrates the reduction from Fe^{3+}–N to Fe^{2+}–N species [41].

The future developments at the BACH beamline aim at implementation of a suitable flow-cell in the end-station in order to handle the undesired radiation damage and radiolysis. This fluidic cell will be dedicated exclusively to *in-situ/in-operando* XAS measurements similar to already existing set-ups at other synchrotron radiation facilities [42, 43]. The device will be equipped with a three electrodes system to carry out cyclic (CV) voltammetry measurements and to record XAS in total fluorescence yield under applied potentials. The main body of the cell will be made in PEEK in order to warrant a high chemical resistance and good electrical insulation. As in the case of the already tested static cells, the liquid will be sealed with a 100 nm thick 1x1 mm^2 Si_3N_4 membrane coated with a Cr/Au mesh to allow the application of potential.

4. Windowless near ambient reaction cells for photoelectron microspectroscopy

As noted in section 3, working with a sub-micrometer photon beam for illumination of the specimen has a great advantage in developing windowless operando set-ups using small pinholes of properly selected dimensions for isolating the specimen and reaction ambient from the UHV analysis SPEM chamber, imposed for monitoring the emitted photoelectrons. Due to the impedance the gas crossover through such pinholes is impeded and the differential pressure on the two sides of the pihnhole, which is separating the sealed reaction cell from the UHV allows preserving the required vacuum conditions of less than 10^{-5} mbar in the SPEM chamber, while inside the vacuum sealed reaction cell the sample can be exposed to gases upto pressures of 1 mbar, supplied via flexible tubes. [44, 45]. The present set-up available at Elettra for SPEM experiments and sketched in Fig. 4, uses two 500 μm diameter pinholes. As illustrated in Fig. 4 the X-ray ~ 0.1-0.2 μm diameter microprobe beam normal to the sample surface enters through the first pinhole and emitted electrons exit through the second pinhole aligned to the acceptance angle of the hemispherical analyzer. The sample is placed on a heater that allows annealing upto max ~700^0 C and can also be biased through the attached electrical contacts for performing electrochemistry experiments in the desired gas ambient. The calibration of the sample temperature was performed in separate preliminary tests that allows accuracy of 15 degrees.

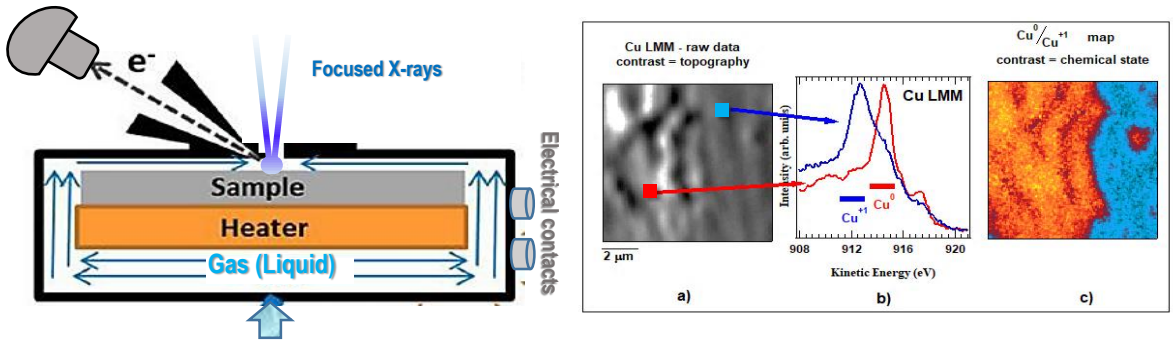

Figure 4: (Left) NAPCell set-up (Right) Representative results a) 12x12 μm^2 SPEM image obtained by collecting the Cu LMM Auger electrons from a partially reduced Cu foil. b): Cu LMM Auger spectra acquired in two different regions of the map indicated by the arrows. c): the ratio of the Cu^0 and Cu^{+1} maps obtained from the raw data image by selecting the maps corresponding to the energy windows indicated in panel b).

This NAPCell was first tested by exploring oxidation and reduction reactions starting with a freshly cleaned and reduced Cu foil. In the first step the Cu^{+1} oxide surface was prepared by exposing the sample to 0.2 mbar O_2 at 350^0 C for one hour. In the next step to attain a partially reduced surface, the oxidized Cu sample was hold in 0.2 mbar H_2 initially at 450^0 C followed by decreasing the temperature to 150^0 C. The two-dimensional maps of the Cu and O photoemission spectra obtained by scanning the sample with respect to the microprobe and the microspot spectra in selected representative areas of the maps reveal the evolution of the surface chemistry and morphology [45]. Fig. 4a) shows a 12x12 μm^2 SPEM image of a partially reduced

Cu surface obtained by collecting the emitted electrons within the Cu LMM Auger energy window. Due to the particular arrangement of the SPEM setup the map contrast is dominated by the surface topography of the unpolished Cu foil. The two representative Cu LMM Auger spectra in Fig. 4b) are acquired in two different regions of the map, as indicated by the two arrows. The red line spectrum corresponds to a fully reduced Cu metallic state, whereas the blue one has the typical lineshape of the Cu^{+1} state. The multichannel detector of the SPEM covering the whole energy window of the Auger spectrum allows selecting the energy windows corresponding to the specific chemical states, as indicated in Fig.4b), and obtain the corresponding Cu^{0} and Cu^{+1} maps [46]. Dividing these two maps to remove the topography contrast we obtain the pure chemical maps shown in Fig. 4c), where the red-yellow indicates the areas of reduced Cu while the blue are the oxidized Cu ones. This model redox reaction experiment illustrates the performance of NAP-SPEM providing a submicron spatial resolution.

This SPEM set-up was recently used for following the evolution at the electrodes of a solid oxide fuel cell operated at 650 C in 0.1 mbar CH_4+O_2 ambient [47]. The chemical maps and micro-spectroscopy measurements at the LSM $(La0.8Sr0.2)0.95MnO_3$) cathode and at the interface with the YSZ $(Y_2O_3)0.08(ZrO_2)0.92$ electrolyte, obtained with lateral resolution of ~150 nm have revealed major changes in the Sr spectra only inside the cathode due to irreversible “lattice” to “surface” Sr segregation. These first SPEM results with SOFC under realistic conditions are very promising for shedding light on the complex chemical and structural changes of operating SOFC that should provide missing information for directing the improvement of these energy devices.

5*. In-situ* and *in-operando* magnetic imaging and spectromicroscopy with PEEM

Photoemission electron microscopy (PEEM) is a full-field type microscopy method that has evolved considerably since the mid ‘90s, finding frequent and successful usage at the third generation synchrotron sources. When collecting secondary electrons for imaging, PEEM can naturally perform X-ray absorption spectroscopy (XAS-PEEM), enabling elemental, chemical and magnetic sensitivity to be combined with full-field microscopy [48]. In conjunction with X-ray magnetic circular or linear dichroism (XMCD or XMLD) PEEM has opened unprecedented opportunities to visualize the magnetic domains in both ferromagnetic and antiferromagnetic materials. Nowadays, XMC/LD-PEEM is an indispensable tool in the study of surface and thin film magnetism [49]. Notable features of the PEEM are the high lateral resolution, which nears ten nm in the best instruments, and the capability to probe buried interfaces. By taking advantage of the pulsed nature of synchrotron light, PEEM can also perform stroboscopic imaging that gives access to the time domain with resolution down to a few tens of picoseconds.

One type of instrument that has become widespread worldwide is the spectroscopic photoemission and low energy electron microscope (SPELEEM), which was introduced at Elettra by Bauer and coworkers [50]. Nanospectroscopy beamline nowadays hosts a more advanced version of the same type of microscope [51, 52]. In brief, the SPELEEM is a hybrid set-up that can perform energy filtered X-ray photoemission electron microscopy (XPEEM) in conjunction with structure sensitive low energy electron microscopy (LEEM) and microspot diffraction (μ-LEED). Its most relevant feature is the ability to provide multiple and complementary methods based on photon and electron probes, as well as imaging in real and reciprocal space [53]. Taking advantage of full-field imaging, the SPELEEM is ideally suited to monitor dynamic processes in real time, such as growth and surface reactions. Several reviews illustrate the previous work carried out at Elettra with this instrument [54, 55, 56]. Here, we will focus primarily on the most recent *in situ* and *in operando* studies.

Due to the high sensitivity to surface structure, LEEM has been frequently employed to follow the preparation of atomically flat layers with desired structural characteristics, as well as to study growth and crystal structure of 2D materials, in particular graphene and metal dichalcogenides [56]. We note that LEEM is not only a characterization tool, but also allows us to actively modify surfaces. Low energy electrons in fact,

just like X-rays, interact with molecular adsorbates, stimulating their desorption and/or dissociation. As a matter of fact, the beam-sample interactions may be detrimental to the chemical stability of the surface, *e.g.* surface reduction, nucleation of vacancies can occur on oxides [57]. Nonetheless, beam stimulated processes can also be exploited to locally modify the surface properties in a desired manner. The concept of this type of experiment dates back to 2006, in a study where micro-focused, low energy electron and x-ray beams were used to locally reduce the rutile TiO_2 surface, where the graft spots of varying density of oxygen vacancies were strongly affecting the subsequent growth of Au [58]. In a similar experiment, the LEEM electron probe was used to locally stimulate the dissociative adsorption of NO_2, providing atomic oxygen and resulting in the formation of thick Ag oxide patches on Ag(111) [59].

By applying a similar in-situ approach, we recently studied the interaction of CO adsorbed on Co/Re(0001). Our microspot XPS experiments with PEEM enabled direct access to the adsorbates' chemical state and coverage during irradiation. Thanks to the fast data acquisition, we revealed the kinetics of the process, permitting us to evaluate cross sections for CO desorption and dissociation. We found that the prolonged irradiation of the Co surface in CO ambient produces carbon deposits, initially promoting the formation of carbides and subsequently accumulating sp^2 carbon on the surface [60]. Photoelectron spectroscopy was crucially important to demonstrate that these overlayers can be converted to graphene upon a short thermal treatment to 380°C [61].

The beam stimulated fragmentation of CO is basic of the chemo-magnetic lithography approach illustrated in Figure N that we first demonstrated grafting chemo-magnetic patterns on the model system Co/Re(0001) [61]. In the first step (a), the local accumulation of surface carbon (carbidic and graphitic species) is promoted by stimulating CO dissociation with micro-focused beams. Subsequently, molecular CO is desorbed from the non-irradiated surface regions by heating the specimen in UHV at 170 °C (b).

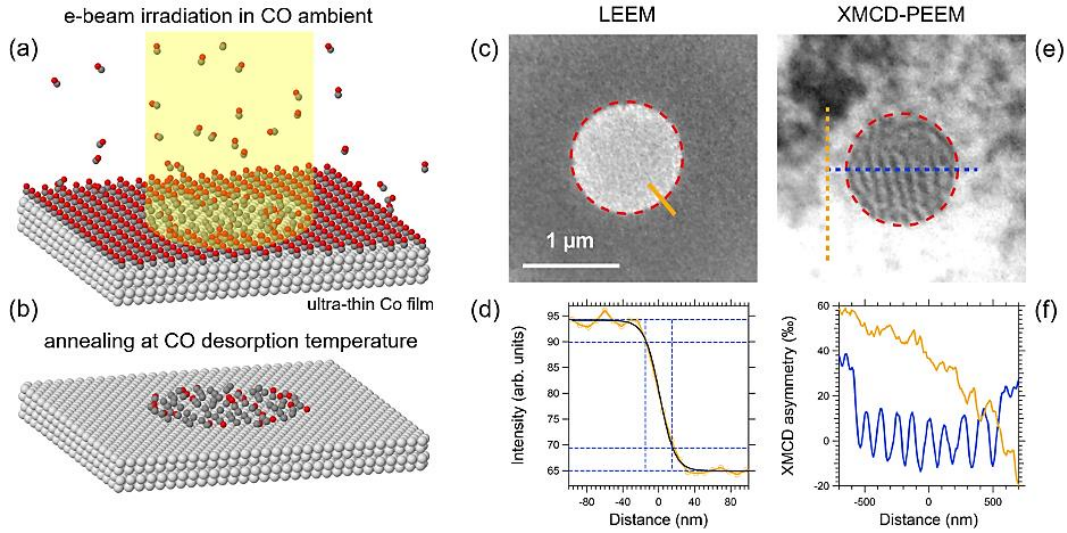

Figure 5. (left) Scheme of the protocol for printing chemo-magnetic patterns in ultrathin Co on Re(0001). (a) The film is exposed to CO at room temperature. The irradiation with a focused electron beam (yellow) stimulates the dissociation of the molecule, which results in the accumulation of atomic carbon on the surface. (b) Subsequently, the sample is annealed above 170 °C to desorb molecularly adsorbed CO from the non-irradiated surface regions. (c) LEEM image of an e-beam irradiated disk. Disk diameter: 1 µm; Co thickness: 4 atomic layers; irradiation energy: 50 eV; CO dose: 9.75 L; (d) Intensity profile across the orange line in the LEEM image in (c) and fit using a step function convoluted with a Gaussian of full width at half-maximum of 30 nm. The dashed blue lines indicate the 15–85% distance between minimum and maximum intensity. (e) XMCD-PEEM image of the same region at the Co L_3 edge. (f) Intensity profiles across the blue and orange dashed lines in the XMCD-PEEM image in (e). The magnetic stripes indicate out-of-plane magnetic anisotropy. The stripe period is 120 nm. Adapted with permission from [61]. Copyright (2018) American Chemical Society.

The chemical patterns grafted using e-beams in CO ambient were characterized using LEEM and XPEEM, which allowed us to correlate the local structure and stoichiometry to the magnetic properties, see Figure 6(c-f). Since the graphitic carbon affects the magnetic properties of the underlying cobalt film due to an electronic effect, resulting in the formation of magnetic patterns, as evidenced by the XMCD-PEEM. The observed striped magnetic domains inside the irradiated area are disclosing the onset of an in-plane to out-of-plane spin reorientation transition occurring in cobalt. The minimum amount of carbon needed to change the magnetic anisotropy of the film is estimated to be about 1/10 of a graphene monolayer. Focusing now on the applications this method can be used to induce confinement effects without destroying the lateral continuity of the Co film. One can thus create and study *in situ* complex, micro-structured magnetic systems, without the need to further process or transfer the sample to a dedicated lithographic set-up.

A further point of interest of the graphene/Co/Re(0001) system is that it exhibits chiral Neél type domain walls, as was revealed by XMCD-PEEM imaging at high lateral resolution. A characteristic image of the domains is shown in Fig. 6, which also provides a fine example of the high lateral resolution of XMCD-PEEM at Elettra. The chirality of the domain walls originates due to strong and asymmetric exchange interactions occurring at the two interfaces of the film, also known as the Dzyaloshinskii–Moriya interaction (DMI). The DMI has been at the center of several exciting developments towards creating magnetic nanostructures, referred to as magnetic skyrmions. Their chiral nature reveals a not trivial topological structure, which reflects the asymmetry of the DMI interaction itself and makes skyrmions robust to external perturbations. Room temperature magnetic skyrmions were first observed in MgO/Co/Pt multilayers using XMCD-PEEM [62].

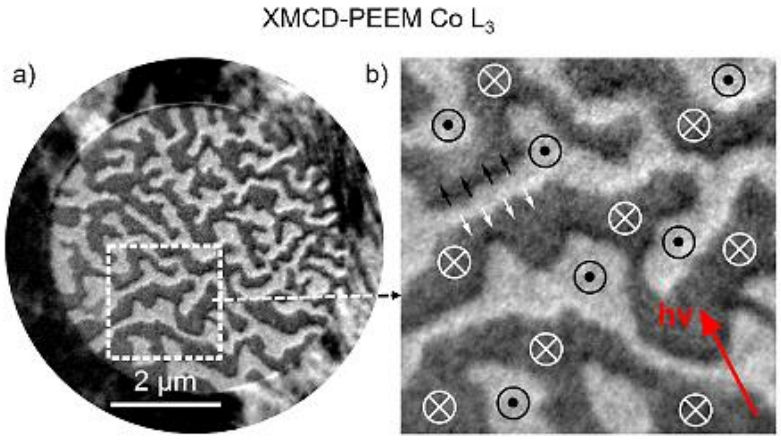

Figure 6. (a) Co L_3 edge XMCD-PEEM image illustrating the magnetic state of ultra-thin cobalt on Re(0001), onto which a disk-shaped graphitic overlayer was printed by e-beam irradiation in CO ambient (the specimen was exposed to a total CO dose of 2700 L) and subsequent thermal treatment at 380 °C. The e-beam irradiated area (at center of the image) exhibits out-of-plane magnetic anisotropy. Its surroundings are magnetized in-plane. (b) Magnified image of the region highlighted by the white dashed square in (a). The out-of-plane domains are separated by chiral Neél walls, revealed by the enhancement in image contrast at the domain boundaries. The red arrow represents the direction of the photon beam; the other symbols indicate the orientation of the magnetization vector. Adapted with permission from [61]. Copyright (2018) American Chemical Society.

The study of nano-magnetism often requires magnetic or electric fields to be applied *in situ* to the specimen, which is especially desirable when addressing the magnetization reversal process. Unfortunately, PEEM is extremely sensitive to such perturbations, since they strongly influence the trajectory of electrons. Experimentally, the application of in-situ fields was solved by building in small coils within the sample holder [63]. Such static fields can reach a maximum value of about 100 Gauss in the out-of-plane direction during imaging, before the misalignment produces a notable degradation in image quality. The Elettra set-up was successfully employed to study *in-operando* the magnetization reversal in graphene-coated Co thin films supported on Re(0001). Magnetic microscopy allowed us to monitor the nucleation of such skyrmion bubbles

in the Co films upon reversing the magnetization with an external field [64]. This observation suggests that under appropriate conditions magnetic skyrmions can be stabilized in graphene/Co/Re(0001).

Another notable application of XMCD-PEEM is the possibility of dynamic imaging of magnetism in cylindrical nanowires. These systems recently attracted large interest, following the observation of exotic magnetic structures identified as Bloch Point Wall (BPW) and Transverse-Vortex Walls (TVW) [65]. These two structures are distinctly different from the topological standpoint, which makes the transformations between the two a matter of interesting dispute. One of the most recent studies regarding the cylindrical wires of soft magnetic materials focused on the field-induced transformations between BPW and TVW using SPELEEM, as well as micro-magnetic simulations [66]. These measurements successfully combined *in-situ* magnetic fields with the shadow XMCD-PEEM method [67] for imaging the internal magnetization distribution in 3-dimensional wires upon application of fields. In the shadow-XMCD measurement a sufficiently small object is illuminated with a focused X-ray beam at a relatively grazing angle, so that the object and its shadow are imaged at the same time. The intensity within the shadow reflects the transmitted X-rays through the bulk of the object. Dichroic signals can be extracted from this transmitted shadow beam, allowing to probe the magnetization in the entire bulk of the nano-object under investigation. Combined with the dichroic signal in the direct photoemission from the object surface, the shadow XMCD provides a means to perform what can be termed as magnetic tomography. Using these unique magnetic probe transformations both from TVW to BPW and from BPW to TVW were observed in the cylindrical nanowires. Micro-magnetic simulations quantitatively reproduced the former, correctly predicting the threshold field at which the transformation occurs. Instead the latter transformation, BPW to TVW, was not seen in the simulations, and it remains an open question, likely to find explanation in the defects (grain boundaries, *etc*.) involved in the actual samples used in the experiments. These results are of great significance, as it constitutes the first report of wall transformations involving nucleation and annihilation of the Bloch Point singularity.

6. Conclusions and Outlook

The presented in this review most recent advances in implementation of experimental set-ups for in-situ/in-operando studies at several Elettra beamlines using photon-in/electron-out spectroscopic and microscopic-imaging approaches have already allowed to uncover various events occurring at functional gas/solid, liquid/solid and solid/solid interfaces imposed to variable working conditions. The presented examples have outlined the crucial importance of surface/near-surface sensitive information obtained under 'working' conditions to investigate phenomena across the sub- micro- to the macroscale.

Great part of the article has been dedicated to illustrate the great advantage of using electron transparent graphene membranes for development of environmental sealed cells for in-operando PES (including also PEEM) that hosts the sample in the desired gas or liquid ambient. We have also demonstrated another great advantage of graphene that placed directly onto the sample can confine a nanometric liquid or gas layer trapped between the graphene membrane and sample surface. Graphene has also excellent transparency for Mid Infrared and Raman and since the interference effect of confined very thin nm water layer is rather weak the on-going developments at Elettra beamlines SISSI and IUVS are focused on implementation of graphene as a water confining layer for studies with micro/nano-IR and micro Raman of hydrated bio-matter, in particular "graphene" liquid cells for multi-technique analysis of living cells in physiological environment [68]. For these studies another advantage of the graphene cover is that it also reproduces exactly the topography of the underlying substance that can be monitored with atomic force microscopy and Nano-IR.

Finally, we would like to notify that there are two important instrumental developments in progress at the Nanospectroscopy facility. Looking towards future machine upgrades that will greatly improve the X-ray beam coherence, we are implementing coherent diffraction imaging (CDI) in reflection geometry within the SPELEEM setup and the first results encoding magnetic dynamics have been obtained [69]. Adding the photon-in/photon-out CDI option to the well-established XPEEM instrument will overcome the common issues related to in-situ application of fields and limited electron escape depth. On another front, in order to

complement the information obtained by XMCD-PEEM, we are developing a magneto-optical Kerr effect (MOKE) set-up with compatible sample stage and UHV transfer to the microscope chamber. Access to MOKE will allow a full magnetic characterization of the samples under investigation.

Acknowledgments

The authors acknowledge financial support from Elettra Sincrotrone Trieste, CNR , MIUR Italy (NFFA , FIRB-RBFR128BEC, ABNANOTECH, FIRB RBAP11ET-KA_0), CERIC-ERIC (RENEWALS) and National Institute of Standards and Technology (NIST) USA.

References

[1] Synchrotron Radiation News, Vol. 30, No. 2, 2017, Special issue on “In-Situ and In-Operando Experiments”.

[2] Ethan J. Crumlin, *J. Electr. Spec. Rel. Phenom.* 200 (2015) 264.

[3] A. Kolmakov, L. Gregoratti, M. Kiskinova, S. Günther, *Topics in Catalysis* 59 (2016) 448.

[4] A. Chakrabarti, M. E. Ford, D. Gregory, R. Hu, C. J. Keturakis, S. Lwin, Y. Tang, Z. Yang M. Zhu M. A. Bañares, I. E. Wachs, *Catalysis Today* 283 (2017) 27.

[5] Johnson Matthey Technol. Rev. 62 (2018) 316.

[6] https://www.elettra.trieste.it/elettra-beamlines/ape.html.

[7] B. Bozzini. M. Amati, L. Gregorati, C. Mele, M. Kazemian Abyaneh, M. Prasciolu, M. Kiskinova, *Electrochem. Commun.* 10 (2008) 1680-1683 and references therein.

[8] C. Castán-Guerrero, D. Krizmancic, V. Bonanni, R. Edla, A. Deluisa, F. Salvador, G. Rossi, G. Panaccione, P. Torelli, *Rev. Sci. Instrum. 89* (2018) 54101.

[9] S. Shroeder, G. Moggridge, R. Lambert, T. Rayment, Spectroscopy for Surface Science in Advances in Spectroscopy Vol. 26 (1998) Ed. R. Clark and R. Hester, Chichester: Wiley

[10] F. Borgatti, P. Torelli, M. Brucale, D. Gentili, G. Panaccione, C. C. Guerrero, B. Schäfer, M. Ruben, M. Cavallini, *Langmuir 34* (2018) 3604.

[11] S. S.-Y. Chui, S. M.-F. Lo, J. P. H. Charmant, A. G. Orpen, I. D. Williams, *Science 283* (1999) 1148.

[12] N. C. Jeong, B. Samanta, C. Y. Lee, O. K. Farha, J. T. Hupp, *J. Am. Chem. Soc.* 134 (2012) 51.

[13] C. Prestipino, L. Regli, J. G. Vitillo, F. Bonino, A. Damin, C. Lamberti, A. Zecchina, P. L. Solari, K. O. Kongshaug, S. Bordiga, *Chem. Mater. 18* (2006) 1337.

[14] S. Bordiga, L. Regli, F. Bonino, E. Groppo, C. Lamberti, B. Xiao, P. S. Wheatley, R. E. Morris, A. Zecchina, *Phys. Chem. Chem. Phys. 9* (2007) 2676.

[15] H. Siegbahn, *J. Phys. Chem.* 89 (1985) 897.

[16] D. F. Ogletree, H. Bluhm, E. D. Hebenstreit, M. Salmeron, *Nucl. Instr. Meth. A:* 601 (2009) 151.

[17] B. Winter and M. Faubel, *Chem. Rev* 106 (2006) 1176.

[18] M. Salmeron and R. Schlogl, *Surf. Sci. Rep.* 63 (2008) 169.

[19] A, Kolmakov, D. A. Dikin, L. J. Cote, J. Huang, M. Kazemian Abyaneh, M. Amati, L. Gregoratti, S. Günther, M. Kiskinova, *Nat. Nanotechnology* 6 (2011) 651.

[20] H. Guo, E. Strelcov, A. Yulaev, J. Wang, N. Appathurai, S. Urquhart, J. Vinson, S. Sahu, M. Zwolak, A. Kolmakov, *NanoLett.* 17 (2017) 1034.

[21] J. Kraus, R. Reichelt, S. Günther, L. Gregoratti, M. Amati, M. Kiskinova, A. Yulaev, I. Vlassiouk, A. Kolmakov, *Nanoscale* 6 (2014) 14394.

[22] A. Yulaev, H. Guo, E. Strelcov, L. Chen, I. Vlassiouk, A. Kolmakov, *ACS Appl. Mat.Interf.* 9 (2017) 26492.

[23] S. Nemšák, E. Strelcov, H. Guo, B. D. Hoskins, T. Duchoň, D. N. Mueller, A. Yulaev, I. Vlassiouk, A. Tselev, C. M. Schneider, A. Kolmakov, *Topics in Catalysis* 61 (2018) 2195.

[24] https://www.elettra.trieste.it/it/lightsources/elettra/elettra-beamlines/esca-microscopy/esca-microscopy.html

[25] M. Krueger, S. Berg, D’Arcy Stone, E. Strelcov, D. A. Dikin, J. Kim, L. J. Cote, J. Huang, A. Kolmakov, *ACS Nano 5* (2011) 10047.

[26] D. Stoll and A. Kolmakov, *Nanotechnology* 23 (2012) Art. no. 505704.

[27] L. Nguyen, P. P. Tao, H. Liu, M. Al-Hada, M. Amati, H. Sezen, L. Gregoratti, Yu Tang, S. D. House, F. F. Tao, *Langmuir,* 34 (2018) 9606.

[28] J. Velasco-Velez, V. Pfeifer, M. Hävecker, R. S. Weatherup, R. Arrigo, C-H. Chuang, E. Stotz, G. Weinberg, M. Salmeron, R. Schlögl, A. Knop-Gericke, *Angew. Chem. Int. Ed*. 54 (2015) 14554.

[29] R. S. Weatherup, B. Eren, Y. Hao, H. Bluhm, M. B. Salmeron, *J. Phys. Chem. Lett.* 7 (2016) 1622.

[30] S. Nappini, A. Matruglio; D. Naumenko, S. Dal Zilio, F. Bondino, M. Lazzarino, E. Magnano, *Nanoscale* 9 (2017) 4456.

[31] A. Yulaev, A. Lipatov, A. X. Lu, A. Sinitskii, M. S. Leite, A. Kolmakov, *Adv. Mat. Interf.* 4 (2017) Art. no. 1600734.

[32] G. Zamborlini, M. Imam, L. L. Patera, T. O. Menteş, N. Stojić, C. Africh, A. Sala, N. Binggeli, G. Comelli, A. Locatelli, *NanoLett.* 15 (2015) 6162.

[33] Q. Fu and X. Bao, *Chemical Society Reviews,* 46 (2017) 1842-1874.

[34] L. Nguyen**,** P. Tao**,** H. Liu**,** M. Al-Hada**,** M. Amati**,** H. Sezen**,** Yu Tang **[a],** L. Gregoratti, F. Tao, *Chem. Commun.* 54 (2018) 9981.

[35] S. Nemšák, E. Strelcov, T. Duchoň, H. Guo, J. Hackl, A. Yulaev, I. Vlassiouk, D. N. Mueller, C. M. Schneider, A. Kolmakov, *J. Amer. Chem. Soc.* 139 (2017) 18138.

[36] https://www.elettra.trieste.it/elettra-beamlines/bach.html

[37] A. Fujishima, X. Zhang, D. A. Tryk, *Int. J. Hydrog. Energy*, 32 (2007) 2664.

[38] A. Fujishima and K. Honda, *Nature*, 238 (1972) 37.

[39] A. Šuligoj, U. L. Štangar and N. N. Tušar, *Chem. Pap.* 68 (2014) 1265.

[40] J. Tang, J. R. Durrant, and D. R. Klug, *J. Am. Chem. Soc.* 130 (2008) 13885.

[41] S. Nappini, A. Matruglio, D. Naumenko, S. Dal Zilio, M. Lazzarino, F.M. F. De Groot, C. Kocabas, O. Balci, E. Magnano, *J. Phys. Chem. C,* 121 (2017) 22225.

[42] D. K. Bora, P.-A. Glans, J. Pepper, Y.-S. Liu, C. Du, D. Wang and J.-H. Guo, *Rev. Sci. Instr*. **85** (2014) 043106.

[43] C. Schwanke, R. Golnak, J. Xiao and K. M. Lange, *Rev. Sci. Instrum.* **85**, (2014) 103120.

[44] H. Sezen, B. Alemán, M. Amati, M. Dalmiglio, L. Gregoratti, *ChemCatChem* 7 (2015) 3665.

[45] H. Sezen, Al-Hada M, Amati M, L. Gregoratti, *Surf. Int. Anal*. 50 (2017) 921.

[46] L. Gregoratti, A. Barinov, E. Benfatto, G. Cautero, C. Fava, P. Lacovig, D. Lonza, M. Kiskinova, R. Tommasini, S. Mähl, W. Heichler, *Rev. Sci. Instr.* 75 *(2004)* 64.

[47] B. Bozzini, D. Kuscer, S. Drnovšek, M. Al-Hada, M. Amati, H. Sezen, L. Gregoratti, *Topics in Catalysis* 20 (2018) 2185.

[48] E. Bauer, Surface Microscopy with Low Energy Electrons; Springer: New York, 2014.

[49] X.M. Cheng, D.J. Keavney. *Rep. Prog. Phys*. 75 (2012) 26501.

[50] T. Schmidt, S. Heun, J. Slezak, J. Diaz, K. Prince, G. Lilienkamp, E. Bauer, *Surf. Rev. Lett.* 05 (1998) 1287.

[51] A. Locatelli, L. Aballe, T.O. Menteş, M. Kiskinova, E. Bauer, *Surf. Interf. Anal.* 38 (2006) 1554.

[52] T. O. Menteş, G. Zamborlini, A. Sala, A. Locatelli, Beilstein *J. Nanotechnol.* 5 (2014) 1873.

[53] T. O. Menteş and A. Locatelli, *J. Electr. Spectr. Relat. Phenom.* 185 (2012) 323.

[54] A. Locatelli and M. Kiskinova, *Chemistry - A European Journal* 12 (2006) 8890.

[55] A. Locatelli and E. Bauer, *J. Phys. Cond. Matter* 20 (2008) 093002.

[56] A. Locatelli and T.O. Menteş, in Synchrotron Radiation, S. Mobilio et al. (eds.); Springer-Verlag Berlin Heidelberg, 2014.

[57] S. Günther, A. Kolmakov, J. Kovac, M. Kiskinova, *Ultramicroscopy* 75 (1998) 35– 51.

[58] T.O. Menteş, A. Locatelli, L. Aballe, A. Pavlovska, E. Bauer, T. Pabisiak, A. Kiejna, *Phys. Rev. B* 76 (2007) 155413.

[59] S. Günther, R. Reichelt, J. Wintterlin, A. Barinov, T.O. Menteş, M.Á. Niño, A. Locatelli, *Appl. Phys. Lett.* 93 (2008) 233117.

[60] F. Genuzio, P. Genoni, T.O. Menteş, B. Santos, A. Sala, C. Lenardi, A. Locatelli, *J. Phys. Chem. C* (2018) Article ASAP; doi: 10.1021/acs.jpcc.8b09043.

[61] P. Genoni, F. Genuzio, T.O. Menteş, B. Santos, A. Sala, C. Lenardi, A. Locatelli, *ACS Appl. Mat. & Interf.* 10 (2018) 27178.

[62] O. Boulle et al, *Nat. Nanotech.* 11 (2016) 449.

[63] M. Foerster, J. Prat, V. Massana, N. Gonzalez, A. Fontsere, B. Molas, O. Matilla, E. Pellegrin and L. Aballe, *Ultramicroscopy* 171 (2016) 63.

[64] F. Genuzio, T.O. Menteş, A. Locatelli, *IEEE Transactions on Magnetics* 55 (2019) 1.

[65] S. Da Col, et al, *Phys. Rev. B* 8 (2014) 180405(R).

[66] A. Wartelle et al, *Phys. Rev. B* 99 (2019) 24433.

[67] S. Jamet et al, *Phys. Rev. B 92* (2015) 144428.

[68] A. Matruglio,a P. Zucchiatti, G. Birarda, B. Marmiroli, F. D'Amico, C. Kocabas, M. Kiskinova, L. Vaccari**,** *J. Instr.*13 (2018) p. C05016.

[69] T. O. Menteş et al, in preparation.

Final published version of this article: Journal of Electron Spectroscopy and Related Phenomena,
Volume 257, 21 October 2019,
Available online: 2 December 2019
DOI: 10.1016/j.elspec.2019.146902